Time stretching of the GeV emission of GRBs: Fermi-LAT data vs geometrical model

Maxim S. Piskunov[1,2] and Grigory I. Rubtsov[2]

Faculty of Physics, Moscow State University, Moscow, Russia

Institute for Nuclear Research of the RAS, Moscow, Russia

maxit@ms2.inr.ac.ru

grisha@ms2.inr.ac.ru

---

[1]Faculty of Physics, Moscow State University, Moscow, Russia.

[2]Institute for Nuclear Research of the RAS, Moscow, Russia.

ABSTRACT

It is known that the high energy ($> 100\,\mathrm{MeV}$) emission of gamma-ray bursts is delayed with respect to the low energy emission. However, the dependence of light curves on energy has not been studied for the high energy bands. In this paper we consider the bursts observed by Fermi LAT from 2008 August 4 to 2011 August 1, for which at least 10 photons were observed with the energy greater than $1\,\mathrm{GeV}$. These include 4 bursts: GRB 080916C, GRB 090510, GRB 090902B, and GRB 090926A. We use the Kolmogorov-Smirnov test to compare the light curves in the two bands, $100\,\mathrm{MeV} < E < 1\,\mathrm{GeV}$ and $E > 1\,\mathrm{GeV}$. For GRB 080916C and GRB 090510 the light curves in the two bands are statistically compatible. However, for GRB 090926A, the higher-energy light curve is stretched compared to the lower-energy one with a statistical significance of 3.3σ and, for GRB 090902B, on the contrary, the lower-energy curve is stretched with 2.3σ significance. We argue that the observed diversity of stretching factors may be explained in a simple geometrical model. The model assumes that the jet opening angle depends on the emission energy in a way that the most energetic photons are radiated near the axis of the jet. All the bursts are considered equivalent in their rest frames and the observed light curves differ only due to different redshifts and view directions. The model conforms to the total burst energy constraint and matches the Fermi-LAT observations of the fraction of GRBs visible in $100\,\mathrm{MeV} < E < 1\,\mathrm{GeV}$ band, which may be observed at higher energies. The model predicts the distribution of observable stretching factors, which may be tested in the future data. Finally, we propose a method to estimate observer's off-axis angle based on the stretching factor and the fraction of the high-energy photons. The code for modeling is open source and is publicly available on GitHub (`https://github.com/maxitg/GammaRays`).

Subject headings: gamma-ray burst: general — gamma-ray burst: individual(GRB 080916C, GRB 090510, GRB 090902B, GRB 090926A)

1. Introduction and summary

Gamma-ray bursts (GRBs) are among the most energetic events in the Universe. Therefore, the studies of the emission mechanism and phenomenology of GRBs may provide the new knowledge in particle physics. Moreover, the GRBs are observed from cosmological distances and therefore bear an imprint of the late-time evolution of the Universe. An extensive studies of these explosions led to a number of interesting results, see Vianello (2012); Gehrels & Razzaque (2013) for a review. **In particular, there are indications that the total energy emitted in gamma-rays during a burst is similar for the different GRBs within an order of magnitude (Postnov et. al. 1999; Bloom et al. 2003; Goldstein et al. 2015). One should keep in mind, though, that there is no agreement on the width of the distribution, and it is in fact model dependent. More recent results, for example, suggest that energetics of different bursts might be different (Racusin et. al. 2009; Chandra & Frail 2012). In this paper, however, we explore the possibility that most of the bursts have similar energetics in their rest frames to simplify analysis. When more precise energy distribution becomes available, the analysis in this paper may be improved. Also, it is generally accepted that the high energy radiation of GRBs follows the predictions of the synchrotron radiation scenario (Wang et al. ApJ)**, although **there are problems with that model (Daigne et al. 2011) and there are bursts in which additional radiation component clearly appears (Abdo et al. 2009).** Several observations are related to the temporal variations of spectra. This way, the spectral lags were found between different low energy bands **(Cheng et al. 1995; Wu & Fenimore 2000)** and the very-high-energy radiation was discovered to be extended relative to the x-ray emission (Castignani et al. 2014; Lange & Pohl 2013; Vianello 2012). In this paper we go further and compare the temporal extension of GRB gamma-ray radiation in the two energy bands $100\,\mathrm{MeV} < E < 1\,\mathrm{GeV}$ and $E > 1\,\mathrm{GeV}$ (hereafter, low and high-energy

bands) using the data from the Large Area Telescope (LAT) of the Fermi satellite (Atwood et al. 2009; Ackermann et al. 2012).

We start with the location, time and duration of bursts from the Fermi-LAT Gamma-Ray Burst Catalog (Ackermann et al. 2013). The photons during the burst and the photons for 24 hours before the burst are downloaded from the LAT Data Server [1]. The latter are used for the background estimation in both energy bands with the technique introduced in Rubtsov et al. (2012). In order to have enough statistics we require that at least 10 photons are detected with the energy greater than $1\,\mathrm{GeV}$. This leaves us with the four bursts for the time span of the Fermi-LAT Gamma-Ray Burst Catalog. Namely, GRB 080916C (Tajima 2009), GRB 090510 (Ackermann et al. 2010), GRB 090902B (Abdo et al. 2009) and GRB 090926A (Ackermann et al. 2011). For these bursts we stretch the high energy light curve by the arbitrary factor and compare with the low energy light curve using the Kolmogorov-Smirnov (KS) test. Within the 95% confidence level the stretching factor is compatible to 1 (no stretching) for the GRB 080916C and GRB 090510. For the other two bursts the stretching factor of 1 is, however, excluded. For GRB 090902B it should be smaller than 1, so the low energy light curve is stretched with respect to the high energy one, see fig. 5. Even more significant deviation from the stretching factor of 1 in the opposite direction is observed for the GRB 090926A. The high energy light curve of GRB 090926A is stretched with respect to the low energy one by a factor of at least 1.99 (see fig. 6). The stretching of the GRB 090926A high energy light is found with 3.3σ significance. All the observed stretching factors are summarized in Table 2, and the detailed procedure for their calculation is described in Section 2.

We propose that the observed energy dependence of the time profiles may be explained without introduction of the new effects. We argue that the stretching may originate from

---

[1]`http://fermi.gsfc.nasa.gov/cgi-bin/ssc/LAT/LATDataQuery.cgi`

the effects of the jet geometry called curvature effects. These effects were explored by multiple authors (**Meszaros et al. 1998; Soderberg 2001; Nakamura & Ioka 2001; Shen et al. 2005; Shenoy et al. 2013; Granot et al. 2002**). **These studies either considered the homogeneous distribution of radiation sources throughout the jet, or assumed dependence of energy and Lorentz factor on the opening angle. The model of this paper is based on a similar assumption that the highest energy radiators are concentrated near the axis of the jet and consequently the jet opening angle depends on energy. The latter is motivated by observations if all bursts are considered equivalent. In this case the energy dependence of the jet opening angle resolves the contradiction between the small fraction of GRBs visible above GeV and the hard spectrum. We assume the Lorentz factor to be constant throughout the jet for simplicity.**

The basic idea of the model is illustrated in Figure 1. The model explains both the stretching factors lower and higher than 1 with the difference of the position of the observer with respect to the burst. The sample light curves are shown in Figure 2. The detailed calculations show that the stretching factors of GRB 090902B and GRB 090926A appear naturally in the model. The predicted distribution of stretching factors is shown in Figure 7.

The rest of the paper is organized as follows. We describe the Fermi LAT data and the analysis procedures in Section 2. The model and the details on calculations are explained in Section 3. The Section 4 introduces three phenomenological tests for the model. The parameters of the model and the new method for estimating the jet observation angles are shown in Section 5. The code for modeling is open source and is publicly available on GitHub (`https://github.com/maxitg/GammaRays`).
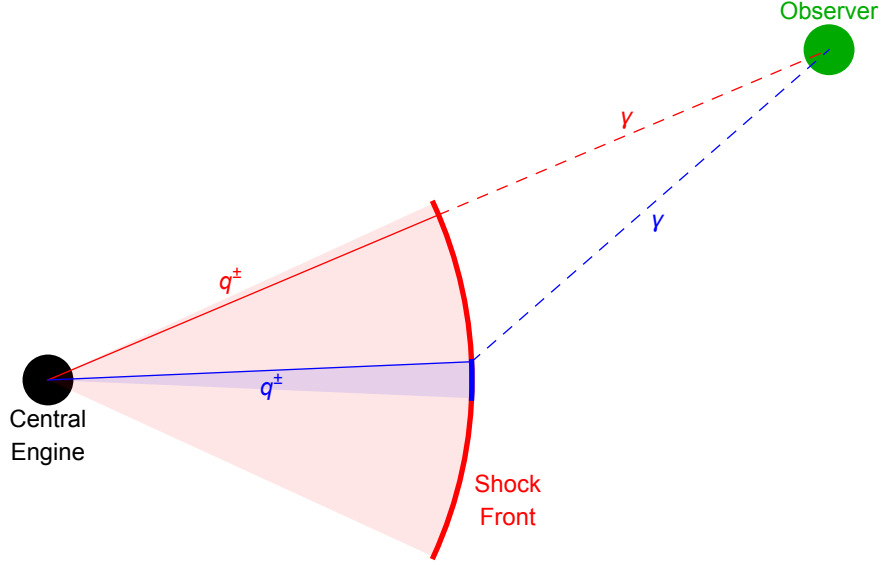
Fig. 1.—: Model Overview. The red and blue cones represent the regions through which low and high energy charged particles propagate. In the case shown the observer's off-axis angle is smaller than the opening angle of the low energy jet, so, due to the relativistic beaming effect, the most of the observable low energy photons will travel along the straight line from the central engine. Also, the observer's off-axis angle is larger that the opening angle of the high energy jet, but the high energy radiation will still originate near the center of the jet as this is the only place where the high energy radiators are located. The observation time of a photon is a sum of two terms. First, the time interval spent in plasma as a radiator which approximately equals to the distance from the central engine to the point of emission. Second, the time interval from emission to detection which equals to the distance from the point of emission to the observer's location. For the given position of the observer the sum is larger for high energy photons. Therefore, the high energy emission will be observed later throughout the burst duration and the high energy light curve will be stretched.

2. Data analysis

2.1. Fermi-LAT Photon Selection

First, we download the Pass 7REP (V15) "SOURCE" class photons from the Fermi-LAT data server (Atwood et al. 2009; Ackermann et al. 2012). In order to define the regions of interest we use the catalog (Ackermann et al. 2013), which contains all the bright gamma-ray bursts seen by the Fermi LAT since 2008 August 4 to 2011 August 1. Specifically, we take 4 pieces of information from the tables 2 and 4 of Ref. Ackermann et al. (2013):

- GBM trigger time. It is used as a reference point for the GRB time.

- Location of the GRB. The burst locations are used to filter out photons coming from the other sources.

- Location error. Location errors are used to improve the accuracy of filtering, specifically to avoid losing statistics by filtering too much.

- $T_{05} - T_{95}$ interval of the LAT-detected emission. The beginning of the interval is used as a fixed point of stretching. The Fermi-LAT photons are downloaded for the period extended in time by 50% towards both past and future compared to this interval.

The data are summarized in Table 1. For the background estimation, we also download observational data for 24 hours before the burst. The analysis is performed with the Fermi Science Tools v9r33p0 package [2] following the guidelines [3]. We require Earth zenith angle

---

[2]http://fermi.gsfc.nasa.gov/ssc/data/analysis/scitools/overview.html

[3]http://fermi.gsfc.nasa.gov/ssc/data/analysis/scitools/data_preparation.html

GRB Name	GBM Trigger Time MET, sec	R.A. J2000, deg	Dec. J2000, deg	Location Error deg	T_{05} sec	T_{95} sec
080825C	241366429.105	233.9	-4.5	0.75	3.2	29.4
080916C	243216766.614	119.85	-56.64	0.0001	5.0	209.8
081006	244996175.173	136.32	-62.05	0.52	0.7	115.0
081024B	246576161.864	322.95	21.2	0.22	0.1	191.0
090217	256539404.560	204.83	-8.42	0.35	6.2	68.0
090323	259459364.630	190.71	17.053	0.0001	15.9	293.9
090328	259925808.510	90.67	-41.715	0.0002	18.8	652.9
090510	263607781.971	333.55	-26.583	0.0004	0.6	45.6
090626	267683530.880	170.03	-33.49	0.22	52.2	299.9
090902B	273582310.313	264.94	27.324	0.001	7.7	825.0
090926A	275631628.990	353.4	-66.32	0.01	5.5	225.0
091003	276237347.585	251.52	36.625	0.0005	3.9	452.6
091031	278683230.850	71.49	-57.65	0.23	3.1	206.2
100116A	285370262.240	305.01	14.43	0.17	3.0	141.0
100414A	292904423.990	192.11	8.693	0.0005	17.4	288.6
110120A	317231981.230	61.5	-12.0	0.36	0.5	112.8
110428A	325675112.410	5.59	64.849	0.00001	10.7	407.6
110721A	332916465.760	333.2	-38.5	0.20	0.1	239.0
110731A	333803371.954	280.504	-28.537	0.0001	3.0	24.1

Table 1:: Burst data used in our study taken from Ackermann et al. (2013).

to be below 100° to remove the Earth limb emission. After the basic filtering by `gtselect` and `gtmktime` tools is done we perform more elaborate selection using the point spread function of Fermi LAT, calculated with `gtpsf` tool. We use 300 energy bins from 100 MeV to 300 GeV, and 300 angular bins with maximal angle being 30°. The `gtltcube` tool is used to compute required livetime maps. Note, that we calculate PSFs separately for both conversion types: front and back. We define PSF_{95} as an angular distance from the source containing 95% of the emitted photons. We require that the photon is closer than $PSF_{95} +$ `location.err` to the location of the GRB (see Table 1). The details of the data request and analysis are given in appendix A.

The set will be used for the analysis with the reservation that it unavoidably contains some background photons. We consider the background flux constant in time and estimate it using the data for 24 hours before the burst. In order to calculate the number of background photons we need an exposure map, which will be discussed in the following section.

2.2. Exposure Maps and Background Estimation

The exposure map is computed with the `gtexpcube2` tool. We compute it with 300 energy bins from 100 MeV to 300 GeV. The produced `expcube` files contain exposures as functions of energy and location on the sky. We use trilinear interpolation to compute exposures for all energies and locations. Knowing the exposures, we use the method introduced in the appendix of Rubtsov et al. (2012) to estimate the background for low and high-energy bands. Note, that the "TRANSIENT" class photons are not included in the analysis due to the strong dependence of the background on the spacecraft position. **Therefore, the background we estimate is mostly sky background for the background from misidentification of protons for "SOURCE" class events is**

subdominant. **Sky background remains stable over the period of** 24 **hours, making our estimate valid during the time of the burst.**

2.3. KS-test

Before applying the KS-test we subtract the background, which is considered linear for the duration of the burst:

$$\Phi_i\left(t\right) = \frac{p_i\left(T_1, t\right) - b_i \frac{t - T_1}{T_2 - T_1}}{p_i\left(T_1, T_2\right) - b_i} \tag{1}$$

Here (T_1, T_2) is the time range of observations, $p_i\left(t_1, t_2\right)$ is the number of photons observed in the time range t_1 to t_2 in the i's energy band (i is either low or high for the low and high-energy bands respectively), and b_i is the estimated number of background photons for the time range T_1 to T_2 in the i's energy band.

The number of degrees of freedom used as an input for the KS-test is $p_i\left(T_1, T_2\right) - b_i$. This is lower than the number of independent photons and therefore we are conservative when estimating the probability and significance of the effect. The KS-probabilities are computed for pairs $\Phi_{\text{low}}\left(t\right), \Phi_{\text{high}}\left(\kappa t\right)$ to obtain the allowed ranges for stretching factors κ for a given confidence level.

2.4. Stretching factors

Out of 19 bursts studied, only 4 have at least 10 high energy events remaining after the filtering, and thus eligible for computing the stretching factors. The results of this computation are shown in Figures 3, 4, 5, 6 and Table 2.

Out of these 4 bursts, two (GRB 080916C and GRB 090510) have stretching factors

compatible with $\kappa = 1$ within 2σ range.

GRB 090926A has, however, high energy radiation stretched with respect to low energy radiation (that is $\kappa > 1$). In contrast to that, GRB 090902B has low energy radiation stretched with respect to high energy radiation ($\kappa < 1$).

Therefore we obtained an indication that the stretching factors for observable bursts may take values both larger and smaller than 1.
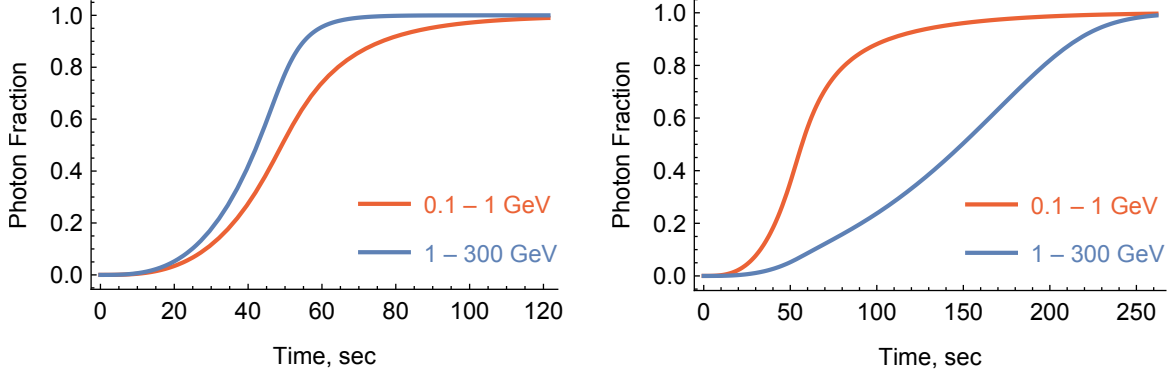
3. Model

The main idea behind our model is to assume that the burst opening angle depends on the energy of emitted photons, or, equivalently, that the most energetic plasma particles are concentrated near the axis of the jet, while low energy particles are on the periphery. As it's seen in Figure 1 this leads to a time stretching effect due to relativistic beaming.

Although the details of the exact mechanism of the GRB are not known there are arguments in support of our model.

First of all, there are around 750 GRBs detected by GBM, half of which are in the LAT field of view at the moment of observation (Vianello 2012). However, only about 30 of them

GRB	1σ		2σ		3σ		4σ		5σ	
080916C	1.04	– 2.24	0.67	– 3.32	0.42	– 5.83	0.19	– 14.9	0.087	– 35.7
090501	0.58	– 1.1	0.43	– 1.61	0.32	– 2.29	0.22	– 3.03	0.17	– 5.11
090902B	0.604	– 0.613	0.35	– 0.89	0.22	– 1.53	0.13	– 2.86	0.078	– 4.49
090926A	2.61	– 3.33	1.99	– 6.62	1.34	– 9.15	0.73	– 13.5	0.48	– 19.4

Table 2:: The ranges of allowed stretching factors for multiple levels of significance for the GRBs studied.

(a) Stretching factor $\kappa = 0.819$, redshift $z = 1.82$, off-axis angle $\chi = 0$.

(b) Stretching factor $\kappa = 2.43$, redshift $z = 2.106$, off-axis angle $\chi = 5.90 \times 10^{-3}$.

Fig. 2.—: High and low energy light curves produced by the geometrical model. Burst parameter values are the same as discussed in Section 5.1.
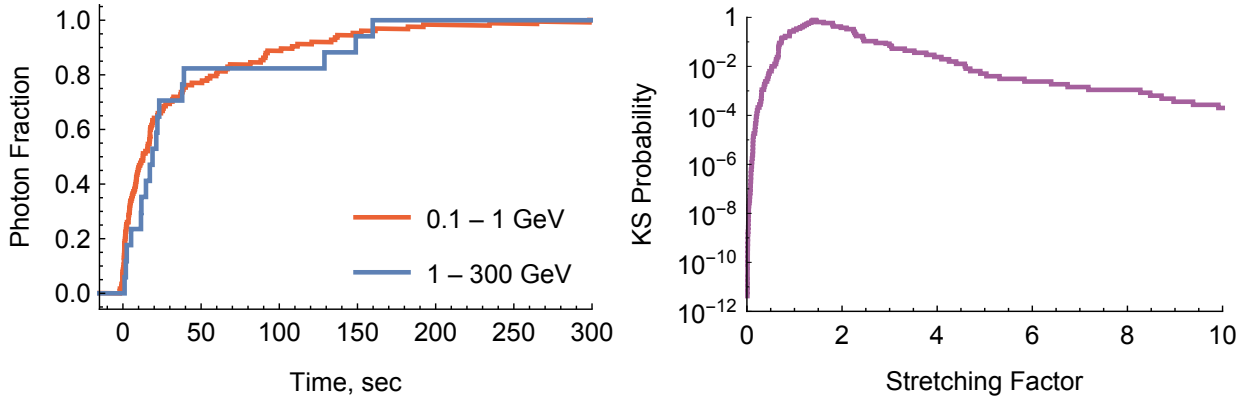

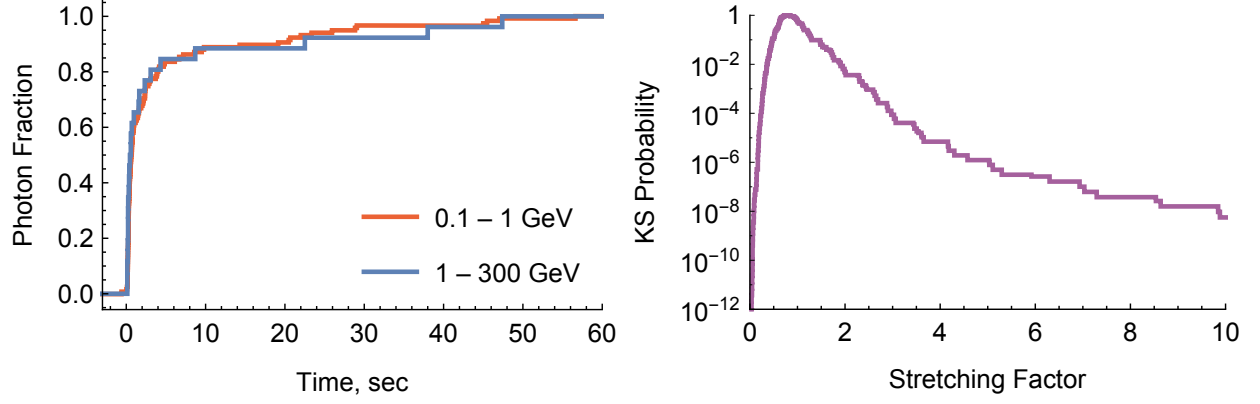Fig. 3.—: GRB 080916C light curves. Stretching factor is compatible with $\kappa = 1$ within 2σ.

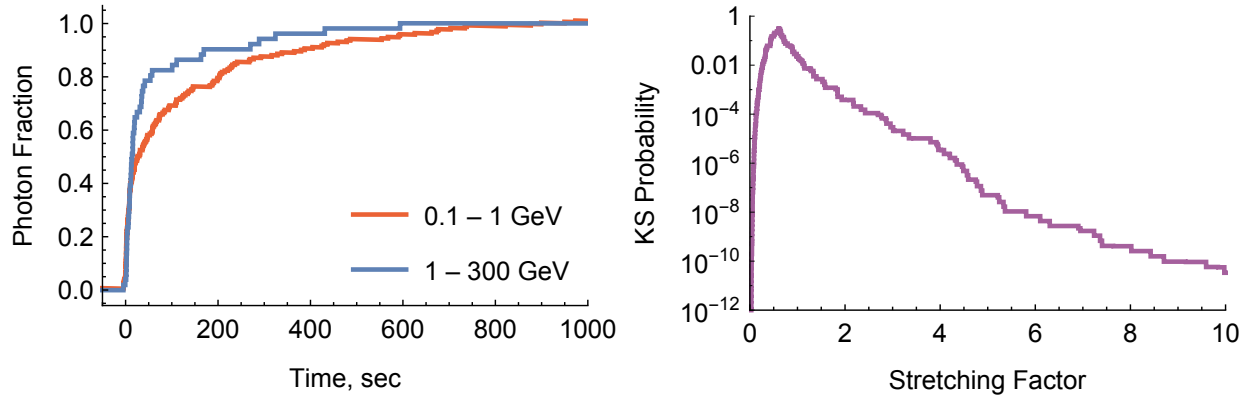Fig. 4.—: GRB 090510 light curves. Stretching factor is compatible with $\kappa = 1$ within 1σ.

Fig. 5.—: GRB 090902B light curves. Low energy radiation is stretched ($\kappa < 1$) with significance of 2.3σ.

were detected by the LAT, and only 4 of them were bright in the high energy band. If one extrapolates the uniform jet model to the very high energies, this observation would mean that these groups of bursts are internally different: some of them produce VHE radiation, while the others do not. **The particular reason for these differences is not known. Explanations may include additional spectral components and variations of the spectra or jet Lorentz factors within GRB population. In this paper we elaborate on explanation, which is not based on the difference of GRB.** The differences in burst counts find natural explanation in our model, in which the opening angle of a jet is inversely proportional to the energy of the photons it radiates. Therefore the most common scenario is that the off-axis angle of an observer is smaller than the low energy jet opening angle, but much larger than the opening angle of a high energy jet. Due to that, most of the bursts can only be seen at low energies. The 4 bursts we study in this paper were seen, according to our model, from the lowest off-axis angles.

Another argument comes from consideration of processes happening in jets, specifically the scattering of particles near the jet boundary. While plasma particles scatter, they simultaneously lose energy, and change directions, sometimes propagating beyond the jet boundary, and therefore increasing the jet opening angle. So, the processes of energy loss and increase of jet size are correlated, therefore the low energy particles should be closer to the jet boundary.

First, let us list the assumptions of the model:

1. Time $t = 0$, a spherical shell of plasma is emitted. The center is called the central engine.

2. The shell points propagate with a constant velocity $v = \frac{\sqrt{\gamma^2 - 1}}{\gamma} \sim 1$, so at the time t the radius of the shall is vt.

3. Each point of the shell is an isotropic radiator in its rest frame.

4. The radiation intensity is a function of the radiator position and the radiation frequency:

$$\eta\left(r, \theta, \omega\right) = \frac{\eta_0}{1 + \left(\frac{r}{r_0}\right)^n} \exp\left(-\left(\frac{\theta}{\theta_0}\right)^2 \left(\frac{\omega}{\omega_0}\right)^{-2k}\right) \left(\frac{\omega}{\omega_0}\right)^\alpha \tag{2}$$

η is a number of particles emitted per volume per solid angle per frequency. It is a function of the distance r from the central engine, of the off-axis angle θ, and of the radiation frequency ω.

The burst is fully defined by the following set of parameters:

- γ, the relativistic factor of the shell, $\gamma \gg 1$.

- η_0, which defines the luminosity scale.

- r_0, the characteristic jet length; $r_0 \ll \frac{1}{H(0)}$, $H\left(t\right)$ is the Hubble parameter;

- n, which determines the sharpness of the jet end, $n > 3$;

- ω_0, a characteristic radiation frequency;

- θ_0, the opening angle of the jet for radiation with frequency ω_0, $\theta_0 \ll 1$;

- k, which determines how much the opening angle changes with frequency, $k < 0$;

- α, the bare spectral index, $\alpha < -2k - 1$

In the next step we calculate the observed light curves, and the stretching factors.

3.1. Photon observation time

We begin with computing a time at which some particular photon is observed. This time is a function of the radiator location (r, θ, ϕ), as well as the observer location $(d, \chi, 0)$ with respect to the burst center (we choose the coordinates so that the rotation angle of the observer is 0.) We assume for now that the observer is too far from the jet to resolve its geometry, yet close enough so that the expansion of space is negligible. The latter assumption is made for simplicity of presentation. The cosmological expansion effect will be restored at the end of this section.

The observation time is a sum of two terms: the time interval from $t = 0$ to the photon emission (the plasma time), and the time interval between the emission and the observation (the photon time):

$$t\left(r, \theta, \phi, d, \chi\right) = t_{\text{plasma}}\left(r\right) + t_{\text{photon}}\left(r, \theta, \phi, d, \chi\right)$$

t_{plasma} is easy to compute since plasma moves with uniform velocity:

$$t_{\text{plasma}}\left(r\right) = \frac{r}{v}$$

t_{photon} is a distance between the radiator and the observer:

$$
\begin{aligned}
t_{\text{photon}}\left(r, \theta, \phi, d, \chi\right) &= \sqrt{\left(d\cos\chi - r\cos\theta\right)^2 + \left(d\sin\chi - r\sin\theta\cos\phi\right)^2 + \left(r\sin\theta\sin\phi\right)^2} \\
&= d\sqrt{\left(\cos\chi - \frac{r}{d}\cos\theta\right)^2 + \left(\sin\chi - \frac{r}{d}\sin\theta\cos\phi\right)^2 + \left(\frac{r}{d}\sin\theta\sin\phi\right)^2} \\
&\sim d\sqrt{\cos^2\chi - 2\frac{r}{d}\cos\theta\cos\chi + \sin^2\chi - 2\frac{r}{d}\sin\theta\cos\phi\sin\chi} \\
&\sim d\left(1 - \frac{r}{d}\left(\cos\theta\cos\chi + \sin\theta\cos\phi\sin\chi\right)\right) \\
&= d - r\left(\cos\theta\cos\chi + \sin\theta\cos\phi\sin\chi\right)
\end{aligned}
$$

Combining these expressions together, we get:

$$t\left(r, \theta, \phi, d, \chi\right) = d + r\left(\frac{1}{v} - \cos\theta\cos\chi - \sin\theta\cos\phi\sin\chi\right)$$

Since no photon can reach the observer faster than the speed of light, and the photons emitted at $t = 0$ reach the observer at $t = d$, this time $t = d$ is the start of the observer's light curve. So we can define a more convenient time origin:

$$\tau\left(r,\theta,\phi,\chi\right) = t\left(r,\theta,\phi,d,\chi\right) - d = r\left(\frac{1}{v} - \cos\theta\cos\chi - \sin\theta\cos\phi\sin\chi\right)$$

Finally, one can use the spherical law of cosines to write this in terms of the great-circle distance $\sigma\left(\theta,\phi,\chi\right)$ between the points (θ,ϕ) and $(\chi,0)$:

$$\tau\left(r,\theta,\phi,\chi\right) = r\left(\frac{1}{v} - \cos\sigma\left(\theta,\phi,\chi\right)\right) \tag{3}$$

Note that τ doesn't depend on d anymore. But this is only true if we did not account for cosmology, or if the scale factor did not change from emission to observation. For a distant observer it will change, however, which will stretch the distances between photons:

$$\tau\left(r,\theta,\phi,z,\chi\right) = r\left(\frac{1}{v} - \cos\sigma\left(\theta,\phi,\chi\right)\right)(1+z) \tag{4}$$

Here z is the redshift of the burst from the point of view of the observer.

3.2. Light curve

We now know enough to compute the observable quantity – the number of observed photons p. For that we need to integrate the radiation intensity η over the four groups of variables. Two groups are burst-related: radiator position (r,θ,ϕ) and frequency at emission ω'. The other two variables are related to observer: observation time τ and frequency at

observation ω. We relate the first two and the second two with the delta functions:

$$p = \frac{A_{\mathrm{det}}}{A_{\mathrm{ph}}(z)} \int_0^\infty \mathrm{d}r \int_0^\pi r\,\mathrm{d}\theta \int_0^{2\pi} r\sin\theta\,\mathrm{d}\phi \int_0^\infty \mathrm{d}\omega' \int_{\tau_1}^{\tau_2} \mathrm{d}\tau \int_{\omega_1}^{\omega_2} \mathrm{d}\omega\, \eta\left(r,\theta,\omega'\right)$$

$$\times \underbrace{\frac{1}{\gamma^2\left(1 - v\cos\sigma\left(\theta,\phi,\chi\right)\right)^2}}_{\text{aberration}} \underbrace{\frac{1}{\gamma\left(1 - v\cos\sigma\left(\theta,\phi,\chi\right)\right)}}_{\text{time dilation}}$$

$$\times\, \delta\left(\frac{\omega'}{\underbrace{\gamma\left(1 - v\cos\sigma\left(\theta,\phi,\chi\right)\right)}_{\text{relativistic shift}}\underbrace{\left(1 + z\right)}_{\text{cosmological shift}}} - \omega\right)$$

$$\times\, \delta\left(\tau - r\left(\frac{1}{v} - \cos\sigma\left(\theta,\phi,\chi\right)\right)\left(1 + z\right)\right) \tag{5}$$

Here A_{det} is the effective area of the detector, and A_{ph} is an area of the sphere over which photons emitted in the burst are spread (see appendix B for derivation). We have taken account for four relativistic effects, which affect intensities and frequencies of the radiators: relativistic aberration; time dilation of the radiators relative to the observer; relativistic blue/redshift; and cosmological redshift.

We integrate over ω' and r using the delta functions. For that we transform them as follows:

$$\delta\left(\frac{\omega'}{\gamma\left(1 - v\cos\sigma\right)\left(1 + z\right)} - \omega\right) = \delta\left(\frac{1}{\gamma\left(1 - v\cos\sigma\right)\left(1 + z\right)}\left(\omega' - \gamma\left(1 - v\cos\sigma\right)\left(1 + z\right)\omega\right)\right)$$

$$= \gamma\left(1 - v\cos\sigma\right)\left(1 + z\right)\delta\left(\omega' - \gamma\left(1 - v\cos\sigma\right)\left(1 + z\right)\omega\right)$$

$$\delta\left(\tau - r\left(\frac{1}{v} - \cos\sigma\right)\left(1 + z\right)\right) = \delta\left(\left(\frac{1}{v} - \cos\sigma\right)\left(1 + z\right)\left(r - \frac{\tau}{\left(\frac{1}{v} - \cos\sigma\right)\left(1 + z\right)}\right)\right)$$

$$= \frac{1}{\left(\frac{1}{v} - \cos\sigma\right)\left(1 + z\right)}\delta\left(r - \frac{\tau}{\left(\frac{1}{v} - \cos\sigma\right)\left(1 + z\right)}\right)$$

After the transformations expression for p takes the following form:

$$p = \frac{A_{\text{det}}}{A_{\text{ph}}(z)} \int_0^\pi d\theta \int_0^{2\pi} d\phi \int_{\tau_1}^{\tau_2} d\tau \int_{\omega_1}^{\omega_2} d\omega$$

$$\times \eta \left(\frac{\tau}{\left(\frac{1}{v} - \cos\sigma(\theta,\phi,\chi)\right)(1+z)}, \theta, \gamma\left(1 - v\cos\sigma(\theta,\phi,\chi)\right)(1+z)\omega \right)$$

$$\times \frac{\tau^2 \sin\theta}{\left(\frac{1}{v} - \cos\sigma(\theta,\phi,\chi)\right)^3 (1+z)^2 \gamma^2 \left(1 - v\cos\sigma(\theta,\phi,\chi)\right)^2}$$

$$= \frac{A_{\text{det}}}{A_{\text{ph}}(z)} \frac{1}{v^2\gamma^2(1+z)^2} \int_{\tau_1}^{\tau_2} d\tau\, \tau^2 \int_0^{\frac{\pi}{2}} d\theta \int_0^{2\pi} d\phi \int_{\omega_1}^{\omega_2} d\omega \frac{\sin\theta}{\left(\frac{1}{v} - \cos\sigma(\theta,\phi,\chi)\right)^5}$$

$$\times \eta \left(\frac{\tau}{\left(\frac{1}{v} - \cos\sigma(\theta,\phi,\chi)\right)(1+z)}, \theta, \gamma\left(1 - v\cos\sigma(\theta,\phi,\chi)\right)(1+z)\omega \right) \qquad (6)$$

Furthermore, one may integrate over ω and τ after using an explicit form for η Eq. 2:

$$p = \frac{A_{\text{det}}}{A_{\text{ph}}(z)} \frac{1}{v^2\gamma^2(1+z)^2} \int_0^\pi d\theta \int_0^{2\pi} d\phi \int_{\omega_1}^{\omega_2} d\omega \int_{\tau_1}^{\tau_2} d\tau\, \tau^2 \frac{\sin\theta}{\left(\frac{1}{v} - \cos\sigma(\theta,\phi,\chi)\right)^5}$$

$$\times \frac{\eta_0}{1 + \left(\frac{\tau}{r_0\left(\frac{1}{v} - \cos\sigma(\theta,\phi,\chi)\right)(1+z)} \right)^n}$$

$$\times \exp\left(-\left(\frac{\theta}{\theta_0}\right)^2 \left(\frac{\omega\gamma\left(1 - v\cos\sigma(\theta,\phi,\chi)\right)(1+z)}{\omega_0} \right)^{-2k} \right)$$

$$\times \left(\frac{\omega\gamma\left(1 - v\cos\sigma(\theta,\phi,\chi)\right)(1+z)}{\omega_0} \right)^\alpha$$

$$= \frac{A_{\text{det}}}{A_{\text{ph}}(z)} \frac{\eta_0}{\left(v\gamma(1+z)\right)^{2-\alpha}} \int_0^\pi d\theta \int_0^{2\pi} d\phi \frac{\sin\theta}{\left(\frac{1}{v} - \cos\sigma(\theta,\phi,\chi)\right)^{5-\alpha}}$$

$$\times \int_{\omega_1}^{\omega_2} d\omega \exp\left(-\left(\frac{\theta}{\theta_0}\right)^2 \left(\frac{\omega\gamma\left(1 - v\cos\sigma(\theta,\phi,\chi)\right)(1+z)}{\omega_0} \right)^{-2k} \right) \left(\frac{\omega}{\omega_0}\right)^\alpha$$

$$\times \int_{\tau_1}^{\tau_2} d\tau\, \tau^2 \frac{1}{1 + \left(\frac{\tau}{r_0\left(\frac{1}{v} - \cos\sigma(\theta,\phi,\chi)\right)(1+z)} \right)^n}$$

$$= \frac{A_{\text{det}}}{A_{\text{ph}}(z)} \frac{\eta_0}{\left(v\gamma(1+z)\right)^{2-\alpha}} \int_0^\pi d\theta \int_0^{2\pi} d\phi \frac{\sin\theta}{\left(\frac{1}{v} - \cos\sigma(\theta,\phi,\chi)\right)^{5-\alpha}}$$

$$\times \left(I(z,\chi,\omega_2;\theta,\phi) - I(z,\chi,\omega_1;\theta,\phi) \right) \left(J(z,\chi,\tau_2;\theta,\phi) - J(z,\chi,\tau_1;\theta,\phi) \right) \qquad (7)$$

Here I and J are indefinite integrals over ω and τ:

$$I(z, \chi, \omega; \theta, \phi) = \frac{\omega \left(\frac{\omega}{\omega_0}\right)^\alpha E_{\frac{\alpha+1}{2k}+1}\left(\left(\frac{\theta}{\theta_0}\right)^2 \left(\frac{\omega}{\omega_0}\right)^{-2k} \left(\gamma\left(1 - v\cos\sigma\left(\theta, \phi, \chi\right)\right)\left(1 + z\right)\right)^{-2k}\right)}{2k}$$

(8)

$$J(z, \chi, \tau; \theta, \phi) = \frac{\tau^3}{3}\, {}_2F_1\left(1, \frac{3}{n}; \frac{n+3}{n}; -\left(\frac{\tau}{r_0\left(\frac{1}{v} - \cos\sigma\left(\theta, \phi, \chi\right)\right)\left(1 + z\right)}\right)^n\right)$$

(9)

where exponential integral function $E_n(x) = \int_1^\infty \frac{e^{-xt}\,\mathrm{d}t}{t^n}$.

The remaining integrals over θ and χ are hard to do symbolically, so we compute them numerically. To optimize this computation we can use the assumption of small θ and χ, so that:

$$\sin\theta \sim \theta$$

$$\cos\sigma\left(\theta, \phi, \chi\right) = \cos\theta\cos\chi + \sin\theta\sin\chi\cos\phi \sim 1 - \frac{\theta^2}{2} - \frac{\chi^2}{2} + \theta\chi\cos\phi$$

Using this assumption, and the evenness of the integral as a function of θ, we arrive to the optimized expressions for p, I and J:

$$p = \frac{A_{\mathrm{det}}}{A_{\mathrm{ph}}(z)} \frac{2\eta_0}{\left(v\gamma\left(1 + z\right)\right)^{2-\alpha}} \int_0^\infty \mathrm{d}\theta \int_0^\pi \mathrm{d}\phi \frac{\theta}{\left(\frac{1}{v} - 1 + \frac{\theta^2}{2} + \frac{\chi^2}{2} - \theta\chi\cos\phi\right)^{5-\alpha}}$$

$$\times \left(I\left(z, \chi, \omega_2; \theta, \phi\right) - I\left(z, \chi, \omega_1; \theta, \phi\right)\right)\left(J\left(z, \chi, \tau_2; \theta, \phi\right) - J\left(z, \chi, \tau_1; \theta, \phi\right)\right) \quad (10)$$

$$I = \frac{\omega \left(\frac{\omega}{\omega_0}\right)^\alpha E_{\frac{\alpha+1}{2k}+1}\left(\left(\frac{\theta}{\theta_0}\right)^2 \left(\frac{\omega}{\omega_0}\right)^{-2k} \left(v\gamma\left(1 + z\right)\left(\frac{1}{v} - 1 + \frac{\theta^2}{2} + \frac{\chi^2}{2} - \theta\chi\cos\phi\right)\right)^{-2k}\right)}{2k} \quad (11)$$

$$J = \frac{\tau^3}{3}\, {}_2F_1\left(1, \frac{3}{n}; \frac{n+3}{n}; -\left(\frac{\tau}{r_0\left(\frac{1}{v} - 1 + \frac{\theta^2}{2} + \frac{\chi^2}{2} - \theta\chi\cos\phi\right)\left(1 + z\right)}\right)^n\right) \quad (12)$$

Finally, we need to compute the limits of p for $\omega_2 \to \infty$ and $\tau_2 \to \infty$. It requires us to

know the limit of I for $\omega \to \infty$ (here we assume that $k < 0$):

$$I\left(z, \chi, \infty; \theta, \phi\right) = \lim_{\omega \to \infty} I\left(z, \chi, \omega; \theta, \phi\right) = 0 \tag{13}$$

and the limit of J for $\tau \to \infty$ ($n > 3$ by assumption):

$$J = \lim_{\tau \to \infty} J\left(z, \chi, \tau; \theta, \phi\right) = \left(r_0 \left(\frac{1}{v} - 1 + \frac{\theta^2}{2} + \frac{\chi^2}{2} - \theta\chi\cos\phi\right)(1+z)\right)^3 \frac{\pi}{n \sin\frac{3\pi}{n}} \tag{14}$$

The following quantities of phenomenological importance may be computed with the use of p:

- the total number of particles observed in a given energy range, $p_\infty\left(z, \chi; \omega_1, \omega_2\right) = p\left(z, \chi; 0, \infty; \omega_1, \omega_2\right)$;

- the fraction of photons observed during a given time interval, $\Phi\left(z, \chi; \tau_1, \tau_2; \omega_1, \omega_2\right) = \frac{p(z,\chi;\tau_1,\tau_2;\omega_1,\omega_2)}{p_\infty(z,\chi;\omega_1,\omega_2)}$;

- the duration of the burst $T_f\left(z, \chi; \omega_1, \omega_2\right)$, that is the time by which the fraction f of photons is observed. One may compute it by solving the following equation for T_f:
$p\left(z, \chi; 0, T_f; \omega_1, \omega_2\right) = f p_\infty\left(z, \chi; \omega_1, \omega_2\right)$;

- the stretching factor, which will be discussed in the next section.

3.3. Stretching factor

The stretching factor for a continuous light curve is defined exactly like the stretching factor for a discrete one. It is the value of κ which makes the KS-distance minimal:

$$\kappa\left(z, \chi; \omega_1, \omega_2, \omega_3\right) = \underset{\kappa}{\operatorname{argmin}} \max_{\tau} \left|\Phi\left(z, \chi; 0, \tau; \omega_1, \omega_2\right) - \Phi\left(z, \chi; 0, \kappa\tau; \omega_2, \omega_3\right)\right| \tag{15}$$

The maximum of an absolute value is not differentiable, so the computation of κ by the given definition is complicated. One may instead rewrite this expression in terms of a positive and a negative KS-distances:

$$D_+ \left(z, \chi; \kappa; \omega_1, \omega_2, \omega_3\right) = \max_\tau \left(\Phi\left(z, \chi; 0, \tau; \omega_1, \omega_2\right) - \Phi\left(z, \chi; 0, \kappa\tau; \omega_2, \omega_3\right)\right)$$

$$D_- \left(z, \chi; \kappa; \omega_1, \omega_2, \omega_3\right) = \min_\tau \left(\Phi\left(z, \chi; 0, \tau; \omega_1, \omega_2\right) - \Phi\left(z, \chi; 0, \kappa\tau; \omega_2, \omega_3\right)\right)$$

$$\kappa \left(z, \chi; \omega_1, \omega_2, \omega_3\right) = \operatorname*{argmin}_\kappa \max \left(D_+ \left(z, \chi; \kappa; \omega_1, \omega_2, \omega_3\right), -D_- \left(z, \chi; \kappa; \omega_1, \omega_2, \omega_3\right)\right)$$

Take note that Φ monotonously increases with τ. It implies that D_+ and D_- monotonously decrease with κ, so as $D_+ + D_-$. So there is a single value of κ, for which

$$D_+ \left(z, \chi; \kappa; \omega_1, \omega_2, \omega_3\right) = -D_- \left(z, \chi; \kappa; \omega_1, \omega_2, \omega_3\right) \tag{16}$$

And this value of κ also makes the $\max\left(D_+, -D_-\right)$ minimal, since D_+ monotonously decrease, and $\left(-D_-\right)$ monotonously increase with κ.

So we arrive at a simpler way to compute κ by solving an equation instead of computing the minimum.

Being able to compute the stretching factor, we could now compare our model predictions with observations given the position of an observer. We don't know the observer's off-axis angle χ, however, so we cannot check the stretching factor prediction on the burst-to-burst basis. Instead, we focus on a series of tests, which will ensure that our model doesn't contradict to existing observations. Namely the test of the total energy and comparison with Fermi-LAT data of the distribution of the stretching factors and the fraction of the high-energy bursts. These tests will be discussed in the following section.

4. Observational tests

4.1. Total energy

In the first test we compute the total energy radiated from the burst, and ensure that it doesn't exceed the mass of the star from which the burst originated.

To compute the total energy, we need to multiply the radiation intensity by frequency, and integrate it over frequencies ω, volume (r, θ, ϕ), and observer positions (σ, ξ). We assume $\theta \ll 1$, and have taken into account the same relativistic effects as we did in the observed particle count computation:

$$
\begin{aligned}
E &= \int_0^\infty d\omega \int_0^\infty dr \int_0^\infty r\, d\theta \int_0^{2\pi} r\,\theta\, d\phi \int_0^\infty d\sigma \int_0^{2\pi} \sin\sigma\, d\xi \\
&\quad \times \eta(r,\theta,\omega) \underbrace{\frac{1}{\gamma(1-v\cos\sigma)}}_{\text{time dilation}} \underbrace{\frac{1}{\gamma^2(1-v\cos\sigma)^2}}_{\text{aberration}} \underbrace{\frac{\omega}{\gamma(1-v\cos\sigma)}}_{\text{relativistic shift}} \\
&= \frac{4\pi^2}{\gamma^4} \int_0^\infty d\omega\, \omega \int_0^\infty dr\, r^2 \int_0^\infty d\theta\, \theta\, \eta(r,\theta,\omega) \int_0^\infty d\sigma \frac{\sin\sigma}{(1-v\cos\sigma)^4}
\end{aligned}
\tag{17}
$$

An integral over σ is computable analytically:

$$
\int_0^\infty d\sigma \frac{\sin\sigma}{(1-v\cos\sigma)^4} = \frac{2(3+v^2)}{3(1-v^2)^3} = \frac{2}{3}\gamma^6\left(4 - \frac{1}{\gamma^2}\right)
$$

Substituting this result into the expression for E we get:

$$
E = \frac{32\pi^2}{3}\left(\gamma^2 - \frac{1}{4}\right) \int_0^\infty d\omega\, \omega \int_0^\infty dr\, r^2 \int_0^\infty d\theta\, \theta\, \eta(r,\theta,\omega)
\tag{18}
$$

Now we can use the expression for η to do the remaining integrals:

$$
\begin{aligned}
E &= \frac{32\pi^2 \eta_0}{3}\left(\gamma^2 - \frac{1}{4}\right) \\
&\quad \times \int_0^\infty d\omega\, \omega \left(\frac{\omega}{\omega_0}\right)^\alpha \int_0^\infty dr \frac{r^2}{1+\left(\frac{r}{r_0}\right)^n} \int_0^\infty d\theta\, \theta \exp\left(-\left(\frac{\theta}{\theta_0}\right)^2 \left(\frac{\omega}{\omega_0}\right)^{-2k}\right)
\end{aligned}
$$

The integrals over r and θ can be computed symbolically:

$$\int_0^\infty dr \, \frac{r^2}{1 + \left(\frac{r}{r_0}\right)^n} = \frac{\pi}{n \sin\left(\frac{3\pi}{n}\right)} r_0^3$$

$$\int_0^\infty d\theta \, \theta \, \exp\left(-\left(\frac{\theta}{\theta_0}\right)^2 \left(\frac{\omega}{\omega_0}\right)^{-2k}\right) = \frac{1}{2}\theta_0^2 \left(\frac{\omega}{\omega_0}\right)^{2k}$$

Now we have only one integral left:

$$E = \frac{16\pi^3}{3n \sin\left(\frac{3\pi}{n}\right)} \left(\gamma^2 - \frac{1}{4}\right) \eta_0 \, r_0^3 \, \theta_0^2 \int_0^\infty d\omega \, \omega \left(\frac{\omega}{\omega_0}\right)^{2k+\alpha} \tag{19}$$

Note, however, that since $\alpha < -2k - 1$ this integral diverges for $\omega \to 0$. This is not a problem as long as our model is not expected to describe low-energy radiation of the burst. One should ensure that the total energy of the high-energy radiation is not too large. For this test, we integrate only over those radiators which emission is observed by Fermi LAT, that is over the frequencies greater than $\frac{\omega_1}{\gamma}$, where ω_1 is the smallest observable photon frequency. Now we compute the last integral and get the final expression for E:

$$E(\omega_1) = \frac{16\pi^3}{3n \sin\left(\frac{3\pi}{n}\right)} \left(\gamma^2 - \frac{1}{4}\right) \eta_0 \, r_0^3 \, \theta_0^2 \int_{\frac{\omega_1}{\gamma}}^\infty d\omega \, \omega \left(\frac{\omega}{\omega_0}\right)^{2k+\alpha}$$

$$= \frac{16\pi^3}{3n \sin\left(\frac{3\pi}{n}\right)} \left(\gamma^2 - \frac{1}{4}\right) \eta_0 \, r_0^3 \, \theta_0^2 \frac{\omega_1^2 \left(\frac{\omega_1}{\gamma\omega_0}\right)^{2k+\alpha}}{\gamma^2(-2k - \alpha - 2)}$$

$$= \frac{16\pi^3}{3n \, (-2k - \alpha - 2) \sin\left(\frac{3\pi}{n}\right)} \gamma^{-2k-\alpha} \left(1 - \frac{1}{4\gamma^2}\right) \eta_0 \, r_0^3 \, \theta_0^2 \frac{\omega_0^{-2k-\alpha}}{\omega_1^{-2k-\alpha-2}} \tag{20}$$

This energy should not exceed a typical mass M_s of a massive star. So, finally, we arrive at the first constraint for the burst parameters:

$$\frac{16\pi^3}{3n \, (-2k - \alpha - 2) \sin\left(\frac{3\pi}{n}\right)} \gamma^{-2k-\alpha} \left(1 - \frac{1}{4\gamma^2}\right) \eta_0 \, r_0^3 \, \theta_0^2 \frac{\omega_0^{-2k-\alpha}}{\omega_1^{-2k-\alpha-2}} < M_s \tag{21}$$

4.2. Distribution of stretching factors

The second test is to calculate the distribution of stretching factors of observable bursts, and to compare it to observations.

The computation of the exact and precise distribution is technically hard and computationally intensive because stretching factor is not a monotonic function of neither redshift nor off-axis angles. We do not compute the distribution directly. Instead, we use the Monte-Carlo method to produce a large representative sample of stretching factors. Then, we calculate an empirical CDF of this sample, which can be compared with observations using the KS-test. Since one may compute much larger sample than that of observations, there is no precision loss due to this simplification.

We still have one ingredient missing though – the evolution of the bursts density. We assume that the bursts density is roughly proportional to the stars density, and the latter is roughly proportional to the matter density, which changes with z as $(1 + z)^3$. It is clear, however, that since no stars existed at very **large** redshifts, the burst density should decline there, so we add an exponential cutoff to it:

$$\rho = \rho_0 \left(1 + z\right)^3 \exp\left(-\frac{z}{z_c}\right) \tag{22}$$

where ρ_0 is a normalization factor, and z_c is a redshift scale, after which the density is cut off.

For the modeling we first need to define the range of redshifts and off-axis angles. The range should include all the observable jet positions, but one should keep the range as small as possible in order to avoid production of too many points corresponding to invisible bursts. For simplicity we consider the rectangular region.

We start with selecting a range for redshifts. Ideally, one would expect that this range starts with $z = 0$. Then, however, there will be visible jets for all possible off-axis angles,

which will make our angles range too large. Note also, that since the bursts count increases with redshift as z^3, the probability to observe a low-redshift burst is very small. So instead of selecting the smallest redshift to be 0, we select it to be a small number $z_{\min} = 0.1$.

$z_{\max}$ is defined by the farthest jet, which can be observed. Since the burst observability $p_\infty(z, \chi; \omega_2, \omega_3)$ decreases with both redshift and χ, we can find the maximum redshift by solving the following equation:

$$p_\infty(z_{\max}, 0; \omega_2, \omega_3) = p_{\min}, \tag{23}$$

where $p_{\min}$ is the minimum number of particles required to claim an observation.

The observability declines with z and χ, so the observable burst with the largest χ should be located at the redshift $z_{\min}$. We can find this angle by solving the similar equation, as we did for the redshifts:

$$p_\infty(z_{\min}, \chi_{\max}; \omega_2, \omega_3) = p_{\min} \tag{24}$$

The simulation is performed by repetition of the following 3 steps before the required number of bursts is attained:

1. First, the random redshift is generated following the distribution 22. This may be done with the Inverse transform sampling method. The CDF of the distribution of redshifts is a ratio of redshift counts in different space volumes:

$$\Phi_z(z) = \frac{\int_{z_{\min}}^z \rho(z') \, dV(z')}{\int_{z_{\max}}^{z_{\max}} \rho(z') \, dV(z')} \tag{25}$$

where $dV(z')$ is the volume of the infinitesimal shell surrounding a sphere over which bursts at redshift z' are distributed (see appendix B for derivation).

To generate a redshift, one should uniformly select a value of Φ_z, and solve the corresponding equation for z:

$$\Phi_z(z) = x \tag{26}$$

where x is a random variable uniformly distributed in the range 0 to 1.

2. The random off-axis angle may be then generated with a similar method. The CDF of the angles distribution is a ratio of spherical areas:

$$\Phi_\chi(\chi) = \frac{\int_0^\chi \sin \chi' \, d\chi'}{\int_0^{\chi_{\max}} \sin \chi' \, d\chi'} \approx \frac{\int_0^\chi \chi' \, d\chi'}{\int_0^{\chi_{\max}} \chi' \, d\chi'} = \left(\frac{\chi}{\chi_{\max}}\right)^2. \tag{27}$$

As with redshifts, we get a properly distributed χ by solving the equation:

$$\Phi_\chi(\chi) = \left(\frac{\chi}{\chi_{\max}}\right)^2 = y, \tag{28}$$

$$\chi = \chi_{\max} \sqrt{y}, \tag{29}$$

where y is an another independent random variable uniformly distributed in the range 0 to 1.

3. Now we check, whether the burst in a selected position may be observed: $p_\infty(z, \chi; \omega_2, \omega_3) > p_{\min}$. If it is, add $\kappa(z, \chi)$ to the sample.

With this algorithm, we arrive to the stretching factor distribution which may be compared with the observed one.

4.3. High energy bursts fraction

Our final test is based on the answer to the following question: given the bursts observed in the whole energy range (ω_1, ω_3), which fraction of them may also be observed in the high energy range (ω_2, ω_3)?

To calculate this ratio, one needs to compute the number of bursts visible in a given

energy range, which is the integral over space and jet directions:

$$b\left(\omega_1, \omega_2\right) = \int_0^{z_{\max}\left(\omega_1, \omega_2\right)} dV\left(z\right) \rho\left(z\right) \int_0^{\chi_{\max}\left(z, \omega_1, \omega_2\right)} 2\pi \sin\chi \, d\chi$$

$$\approx 2\pi \int_0^{z_{\max}\left(\omega_1, \omega_2\right)} dV\left(z\right) \rho\left(z\right) \int_0^{\chi_{\max}\left(z, \omega_1, \omega_2\right)} \chi \, d\chi$$

$$= \pi \int_0^{z_{\max}\left(\omega_1, \omega_2\right)} dV\left(z\right) \rho\left(z\right) \chi_{\max}^2\left(z, \omega_1, \omega_2\right) , \tag{30}$$

where $z_{\max}\left(\omega_1, \omega_2\right)$ and $\chi_{\max}\left(z, \omega_1, \omega_2\right)$ are the same values we used in the previous section: the maximum redshift from which a burst can be observed in a given energy range, and the maximum off-axis angle with which the burst at redshift z can be observed.

The required fraction is the ratio of these integrals:

$$f\left(\omega_1, \omega_2, \omega_3\right) = \frac{b\left(\omega_2, \omega_3\right)}{b\left(\omega_1, \omega_3\right)} = \frac{\int_0^{z_{\max}\left(\omega_2, \omega_3\right)} dV\left(z\right) \rho\left(z\right) \chi_{\max}^2\left(z, \omega_2, \omega_3\right)}{\int_0^{z_{\max}\left(\omega_1, \omega_3\right)} dV\left(z\right) \rho\left(z\right) \chi_{\max}^2\left(z, \omega_1, \omega_3\right)} . \tag{31}$$

Our 3rd test is the comparison of the obtained ratio with the observed value.

5. Results

5.1. Parameter fit

For now we have discussed how to compute various observables of the model, and how to test the model against the data from observations. Now we come to the discussion of specific values for the parameters of the burst.

First of all, we need to determine, which parameters to fit. At most, the observables of a particular burst depend on 10 parameters: 8 of the burst $(\gamma, \eta_0, r_0, n, \omega_0, \theta_0, k, \alpha)$, and 2 of the observer's position related to the burst (z, χ). However, some of these parameters only change observables trivially, and, also, there are transformations of variables, which do not change observables at all (see equation 10):

- The number of photons p depends linearly on η_0, so η_0 doesn't affect other observables like duration, or stretching factor. One can easily fit η_0 to match the observed photon count.

- **If we make a simultaneous transformation of $r_0 \to \lambda_1 r_0$ and $\eta_0 \to \frac{1}{\lambda_1^3}\eta_0$, where** λ_1 is a parameter of transformation, only duration of the burst will change. Other observables, like the total number of photons, or stretching factor, will not be affected.

- **Finally, if we make a following transformation: $\omega_0 \to \lambda_2\omega_0$, $\theta_0 \to \lambda_2^k\theta_0$,** $\eta_0 \to \lambda_2^\alpha\eta_0$, **where** λ_2 is another transformation parameter, no observables will change whatsoever.

Given these transformations, one can reduce the number of parameters for fit to 7: $(\gamma, n, \theta_0, k, \alpha, z, \chi)$.

Also, some of these parameters are known from observations:

- Redshifts z of many bursts have been measured (Ackermann et al. 2013).

- We know that relativistic factors γ are on the order of magnitude[4] of $\gamma = 300$ (Ghirlanda et al. 2012).

This knowledge allows us to reduce the number of parameters to minimize against to just 5: $(n, \theta_0, k, \alpha, \chi)$.

We are going to fit parameters specifically for GRB 090926A for its stretching factor is the most significant. While we assume burst related

---

[4]Our minimization procedure can find similar minimums for other values of γ, at least from 100 to 1000

parameters (n, θ_0, k, α) to be the same for all bursts, χ here considered to be the off-axis angle of GRB 090926A. At the same time, we need to make sure that burst related universal parameters (n, θ_0, k, α) are consistent with observation of other bursts such as GRB 090902B.

In particular, the best fit parameters are found by minimizing the cost function $C(n, \theta_0, k, \alpha, \chi)$ which satisfies the following objectives:

- Total energy of the burst is finite (that is $k + \frac{\alpha}{2} + 1 < 0$) and smaller than $6 \times 10^{53} \, \text{GeV} \approx 10^{51} \, \text{erg}$ (Gehrels & Razzaque 2013).

- The stretching factor of the burst should be compatible with the value for the GRB 090926A.

- The ratio of photons with high energies and low energies should be compatible with the value for the GRB 090926A, $\frac{p_\infty(z, \chi; 1 \, \text{GeV}, \infty)}{p_\infty(z, \chi; 0.1 \, \text{GeV}, 1 \, \text{GeV})} = 0.057$.

- The burst should not be too faint compared to other bursts from the sample. In other words, the total number of observed photons should approximately equal to the median among the sample.

- We assume that all bursts have the same burst parameters $(\gamma, \eta_0, r_0, n, \omega_0, \theta_0, k, \alpha)$ and require that bursts with small stretching factors like GRB 090902B should be possible to observe. So we require that bursts with the stretching factor of GRB 090902B or lower appear in random samples by varying z and χ (sampling is done the same way as in Section 4.2). Note that this requirement unlike others applies to an ensemble of simulated bursts.

The cost function is then computed by the following procedure:

1. Set $\gamma = 300$, $\omega_0 = 1 \, \text{GeV}$, $z = 2.1062$ (which is the redshift of GRB 090926A)

2. Set η_0 and r_0 such that the duration of the burst, and the total number of observed photons are compatible with GRB 090926A, $T_{0.99}(z, \chi; 0.1\,\text{GeV}, \infty) = 219.5\,\text{sec}$ and $p_\infty(z, \chi; 0.1\,\text{GeV}, \infty) = 179.996$

3. If $k + \frac{\alpha}{2} + 1 < 0$, or the energy of the burst $E(0.1\,\text{GeV}) > 6 \times 10^{53}\,\text{GeV}$, the cost function equals to the penalization factor: $C(n, \theta_0, k, \alpha, \chi) = 400$.

4. Compute the small sample of 10 bursts (we will need stretching factors and total photon counts) with the same fixed burst parameters $(\gamma, \eta_0, r_0, n, \omega_0, \theta_0, k, \alpha)$, and with z and χ representatively distributed (as discussed in Section 4.2).

5. Compute the cost due to the stretching factor:

$$C_\kappa = \frac{\log \kappa(z, \chi; 0.1\,\text{GeV}, 1\,\text{GeV}, \infty) - \log \kappa_{\text{GRB090926A}}}{\Delta \log \kappa_{\text{GRB090926A}}} \tag{32}$$

Here $\log \kappa_{\text{GRB090926A}} = \frac{1}{2}\left(\log(6.62) + \log(1.99)\right)$ and $\Delta \log \kappa_{\text{GRB090926A}} = \frac{1}{2}\left(\log(6.62) - \log(1.99)\right)$.

6. Compute the cost due to the fraction of high and low energy photon counts:

$$C_f = \frac{\log \frac{p_\infty(z, \chi; 1\,\text{GeV}, \infty)}{p_\infty(z, \chi; 0.1\,\text{GeV}, 1\,\text{GeV})} - \log f_{\text{GRB090926A}}}{\log(10)} \tag{33}$$

Here $f_{\text{GRB090926A}} = 0.0570003$.

7. Compute the cost due to the brightness of the burst compared to the median:

$$C_b = \frac{\log \frac{p_\infty(z, \chi; 0.1\,\text{GeV}, \infty)}{p_{\text{med}}} - 0}{\log(10)} \tag{34}$$

Here p_{med} is the median number of observed photons among the sample computed in the step 4.

8. Compute the cost due to the minimal stretching factor from the sample:

$$C_{\kappa\text{min}} = \max\left(0, \frac{\log \kappa_{\text{min}} - \log \kappa_{\text{GRB090902B}}}{\Delta \log \kappa_{\text{GRB090902B}}}\right) \tag{35}$$

Here $\kappa_{\min}$ is the minimal stretching factor from the sample computed in the step 4, $\log \kappa_{\text{GRB090902B}} = \frac{1}{2} \left(\log (0.89) + \log (0.35) \right)$ and $\Delta \log \kappa_{\text{GRB090902B}} = \frac{1}{2} \left(\log (0.89) - \log (0.35) \right)$.

9. Finally, the value of the cost function is the sum of squares of the four:

$$C = C_{\kappa}^2 + C_f^2 + C_b^2 + C_{\kappa\min}^2 \tag{36}$$

We use the Nelder-Mead (downhill simplex) method for the minimization procedure. Initial points were chosen to include the areas in parameter space where each cost is close to 0 (first 4 points correspondingly), and to cover the large fraction of the parameter space. You can see the values in Table 3.

The minimization converged to the following parameter values:

- $\gamma = 300$

- $\eta_0 = 4.629640817921788 \times 10^{34} \sec^{-3} \text{GeV}^{-1}$

- $r_0 = 3.142715108207946 \times 10^6 \sec$

- $n = 22.9977$

- $\omega_0 = 1\,\text{GeV}$

- $\boldsymbol{\theta_0 = 7.93393 \times 10^{-5}}$

- $\boldsymbol{k = -0.65356}$

- $\boldsymbol{\alpha = -0.724394}$

- $z = 2.1062$

- $\boldsymbol{\chi = 0.00590163}$

Note, that these parameter values (except for z and χ) are universal, and they may describe the whole population of observed bursts, as will be shown in the next section.
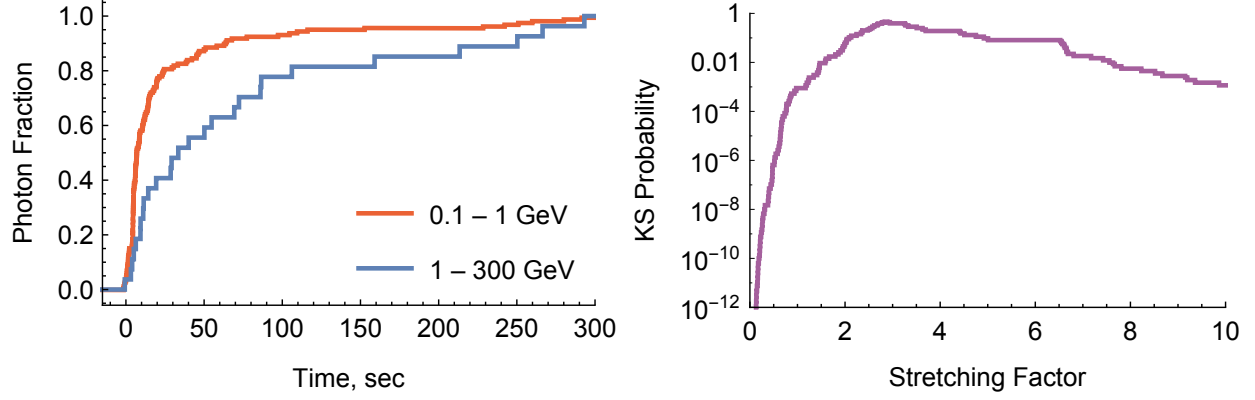
Fig. 6.—: GRB 090926A light curves. High energy radiation is stretched ($\kappa > 1$) with significance of 3.3σ.

n	θ_0	k	α	χ
22.1525	2.16424×10^{-4}	-0.417021	-1.3516300	7.04982×10^{-3}
25.8640	4.90222×10^{-8}	-2.908750	3.5380100	2.86570×10^{-4}
17.5380	1.46284×10^{-3}	-2.133600	-2.1336000	1.52624×10^{-3}
17.9736	4.52631×10^{-6}	-1.402620	-0.0114132	3.25900×10^{-4}
5.0000	1.12535×10^{-7}	-0.200000	-2.0000000	4.73795×10^{-3}
7.0000	2.00000×10^{-12}	-3.000000	-3.0000000	1.73795×10^{-3}

Table 3:: Initial points used for minimization procedure from Section 5.1.

5.2.   Results of the tests

As was discussed in the previous section our model can reproduce both stretching factors smaller than 1 (like of GRB 090902B) and larger than 1 (like of GRB 090926A) depending on redshift and observer's off-axis angle (see fig. 2).

Below are the results of the tests of Section 4:

- The total energy emitted in $100 \, \mathrm{MeV}$ and more energetic gamma rays $E < 5.89 \times 10^{53} \, \mathrm{GeV}$, which is in agreement with Gehrels & Razzaque (2013).

- The distribution of observable bursts' stretching factors is shown in Fig. 7. This distribution does not contradict to the values of stretching factors obtained in Section 2.

- The fraction of bursts observable in low energy band, which are also observed in high energy band is $f_m = 0.110$. The Fermi-LAT catalog contains 35 bursts out of which 4 can be observed in high energy band. Therefore the observed value $f_o = 0.11 \pm 0.05$ (error from binomial distribution) agrees with the model.

Therefore the model successfully explains the variety of the stretching factors observed by the Fermi LAT.

6.   Discussion

The are some caveats and possible directions of improvement of the model. First of all, as it's seen in Fig. 8 the stretching factor of GRB 090926A is higher that the model prediction. More data are needed to understand whether this requires a refinement of the model or is a statistical fluctuation.

Second, the shapes of light curves produced by the model (see fig. 2) differ considerably from observed ones (e.g. fig. 5). In particular, the slope of light curves produced by the model is zero at $t = 0$, while the slope of the observed light curves at $t = 0$ appears to have a maximum.

Third, the assumption of plasma energy dependence on off-axis angle should be better justified. This might probably be done using hydrodynamic simulation of the jet.

We note, that even though it appears that bursts are similar in their rest frames, this may be considered only as a first approximation. The differences in masses, metallicities, angular momenta of progenitor stars, and the differences in local conditions around them might account for differences in light curves of GRBs (or, even, for especially large stretching factor of GRB 090926A). This means that the minor variations of the model parameters might be necessary.

It seems, however, that all the issues above may be addressed by refining the model without changing it's main assumptions.

Our study can be summarized with 3 main conclusions.

First, the time stretching of GRB light curves between different VHE (in particular $100\,\text{MeV} < E < 1\,\text{GeV}$ and $E > 1\,\text{GeV}$) bands is discovered with the statistical significance of 3.3σ. Depending on the burst the stretching factor may be higher or lower than 1, that is the higher or the lower-energy light curve is stretched.

Second, the time stretching may be explained with curvature effects, that is the effects of jet geometry. There is no need to introduce any new spectral components.

Finally, one may assume that all GRBs are the same in their rest frames. The internal burst parameters (such as γ, η_0, r_0, n, ω_0, θ_0, k and α) might stay the same for all bursts, and this assumption is more or less consistent with existing observations.

We note, that the model predicts a correlation between the fraction of the high energy photons, the stretching factor and the observer's off-axis angle (see fig. 8). This may be used as a method to estimate the observer's off-axis angle.

Facilities: Fermi LAT.

A.   Details of using Fermi Science tools

This appendix contains the details on using the Fermi-LAT data. Namely, the exact values passed to the web form on the Fermi-LAT data server and the code used to run the Fermi tools including the full list of options.

Parameters that are passed to the web form of the Fermi-LAT data server to download the bursts data are the following:

- **Object name or coordinates**. Coordinates are filled from the Table 1.

- **Coordinate system**. J2000.

- **Search radius (degrees)**. 60. Events are filtered by location separately by using the point spread functions (PSFs) of the LAT (as described in Section 2.1).

- **Observation dates**. To have a decent safety margin, we extend the duration of the
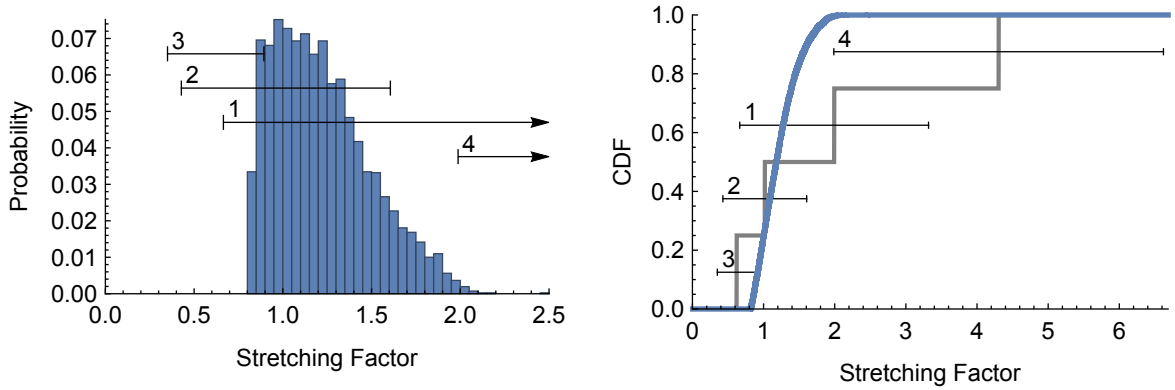
(a) Histogram (blue) obtained from the model. Black error bars show observed stretching factors.

(b) CDF (blue) obtained from the model. Gray curve and black error bars show observed stretching factors.

Fig. 7.—: Stretching factors histogram and CDF produced by our model. The sample contains 4096 bursts. Numbered error bars correspond to GRB 080916C, GRB 090510, GRB 090902B and GRB 090926A (in this order).
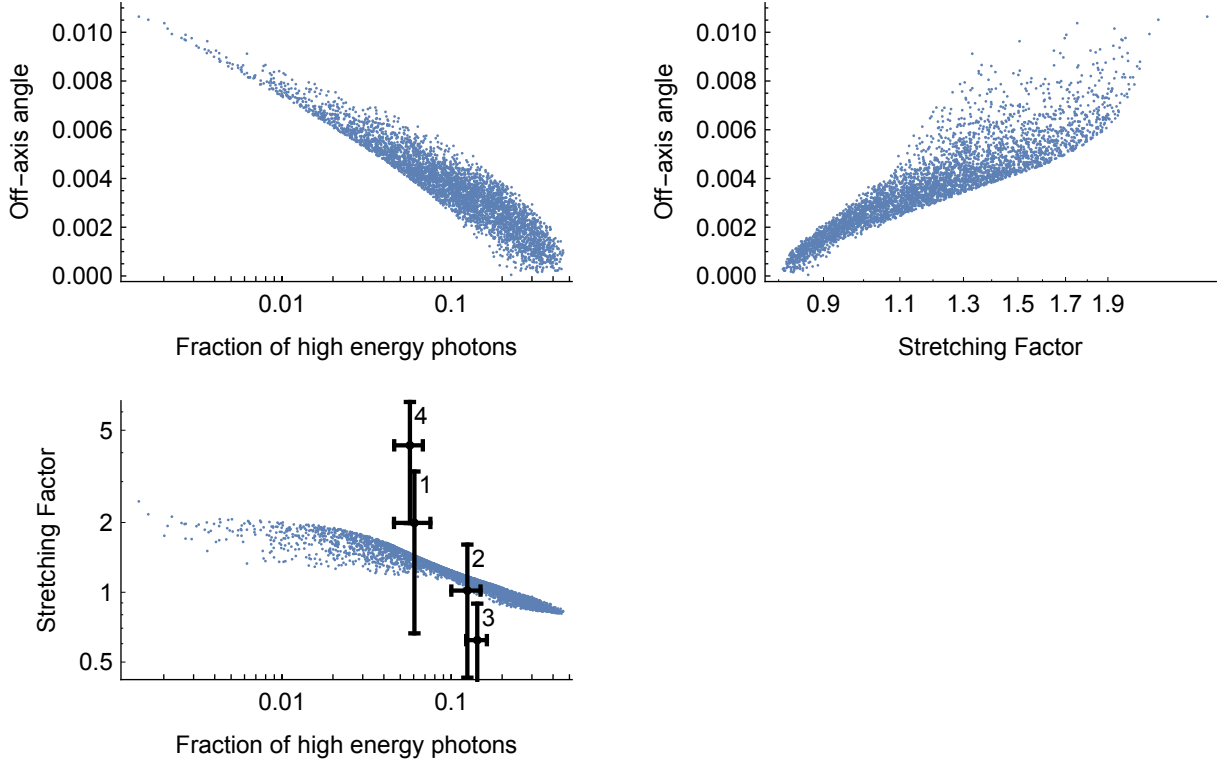
Fig. 8.—: Correlations between off-axis angles, stretching factors and high to low energy photon count ratios found in the sample produced by our model. The sample contains 4096 bursts. Numbered black crosses show data for GRB 080916C, GRB 090510, GRB 090902B and GRB 090926A (in this order) with 2σ error bars. This correlation allows one to estimate off-axis angles of observed bursts.

burst by 50% to both past and future relative to the Table 1 time ranges. So, we fill in the following values:

$$\text{time} + \text{startOffset} - 0.5\,(\text{endOffset} - \text{startOffset}),$$

$$\text{time} + \text{endOffset} + 0.5\,(\text{endOffset} - \text{startOffset})$$

- **Time system**. MET.

- **Energy range (MeV)**. 100, 300000. This includes our both energy ranges.

- **LAT data type**. Extended.

- **Spacecraft data**. Checked. It is required for both events filtering, and calculation of the PSFs and exposure maps.

For background, all the parameters are the same, except for the time ranges, which are the following:

$$\text{time} + \text{startOffset} - 0.5\,(\text{endOffset} - \text{startOffset}) - 86400,$$

$$\text{time} + \text{startOffset} - 0.5\,(\text{endOffset} - \text{startOffset})$$

The commands we use to run the Fermi Science Tools are the following:

```
gtselect  infile=[eventFile]  outfile=filtered.fits
        ra=INDEF  dec=INDEF  rad=180  tmin=INDEF  tmax=INDEF
        emin=100  emax=300000
        zmax=100  evclass=2  convtype=-1  evtable=EVENTS
```

Here [eventFile] is the file downloaded from the Fermi-LAT data server.

```
gtmktime  scfile=[spacecraft]  sctable=SC_DATA
        filter="DATA_QUAL>0 && LAT_CONFIG==1"  roicut=yes
```

```
evfile=filtered.fits  evtable=EVENTS  outfile=timed.fits
apply_fiter=yes
```

where `[spacecraft]` is the FITS file containing the spacecraft data (also downloaded from the Fermi-LAT data server).

```
gtltcube  evfile=timed.fits  evtable=EVENTS
scfile=[spacecraft]  sctable=SC_DATA
outfile=ltcube.fits
dcostheta=0.025  binsz=1  phibins=0
tmin=0  tmax=0  zmax=100  zmin=0
```

```
gtpsf expcube=ltcube.fits  outfile=psf_[IrfName].fits
outtable=PSF  irfs=[IrfName]
ra=[RA]  dec=[DEC]  emin=100  emax=300000
nenergies=41  thetamax=30  ntheta=300
```

`[RA]` and `[DEC]` here are the coordinates of the burst, and `[IrfName]` is the Instrument Response Function, which depends on photon's event class ("SOURCE" in our case) and conversion type (back or front). The list of IRF names is obtained with the `gtirfs` tool.

```
gtexpcube2  infile=ltcube.fits  cmap=none
outfile=expcube_[IrfName].fits  irfs=[IrfName]
nxpix=360  nypix=180  binsz=1  coordsys=CEL
xref=0  yref=0  axisrot=0  proj=CAR
ebinalg=log  emin=100  emax=300000  enumbins=40
ebinfile=NONE  bincalc=EDGE  ignorephi=no
thmax=180  thmin=0  table=Exposure
```

Note, that R.A. coordinates in the `expcube` FITS files are indexed in reverse order and

start from 180. For example, `ra[0]` $= 180$, `ra[1]` $= 179$, and so on.

B.   Cosmological distances

This appendix contains a few formulas related to the cosmological distances. In particular, it provides formula for the area of a photon sphere $A_{\mathrm{ph}}(z)$, a sphere over which photons emitted in a particular burst at redshift z are spread; and the volume of the infinitesimal shell surrounding a burst sphere $\mathrm{d}V(z)$, a sphere over which bursts at redshift z are distributed.

First of all, the metric of the expanding Universe:

$$\mathrm{d}s^2 = -\,\mathrm{d}t^2 + a^2(t)\,\mathrm{d}r^2 + a^2(t)\,r^2\,\mathrm{d}\Omega_2 \tag{B1}$$

We define $a(t_{\mathrm{obs}}) = 1$, where t_{obs} is the observation time.

We need to understand how the scale factor changes with time. For that we assume that the energy content of the Universe consists of matter Ω_m and vacuum energy Ω_Λ only, so that the Friedmann equation takes the following form:

$$\left(\frac{\dot{a}(t)}{a(t)}\right)^2 = \Omega_m H_{\mathrm{obs}}^2 \frac{1}{a^3(t)} + H_{\mathrm{obs}}^2 \Omega_\Lambda$$

$$\dot{a}(t) = a(t)\,H_{\mathrm{obs}}\sqrt{\Omega_m \frac{1}{a^3(t)} + \Omega_\Lambda}$$

$$\mathrm{d}t = \frac{\mathrm{d}a}{a(t)\,H_{\mathrm{obs}}\sqrt{\Omega_m \frac{1}{a^3(t)} + \Omega_\Lambda}}$$

Here $H_{\mathrm{obs}} = H(t_{\mathrm{obs}}) = \frac{\dot{a}(t_{\mathrm{obs}})}{a(t_{\mathrm{obs}})} = \dot{a}(t_{\mathrm{obs}})$ is the Hubble parameter at the observation time.

We also need to know the areas of two spheres: the photon sphere, a sphere over which photons emitted in a particular burst are spread; and the bursts sphere, a sphere over which bursts at a particular redshift are distributed. These two spheres have the same radii – a

distance from the observer to the burst, but different centers: the photon sphere is centered on the burst, while the bursts sphere is centered on the observer. Also, they have different areas, because the scale factor differs at the time of emission and observation.

Let us begin with the photon sphere. This sphere has the origin at $r = 0$ and $t = 0$, at the central engine of a particular burst. Taking $\mathrm{d}s = 0$ and $\mathrm{d}\Omega_2 = 0$ in the equation for metric, we get:

$$\mathrm{d}r = \frac{\mathrm{d}t}{a\,(t)}$$

And now we integrate over time to find the observer's position:

$$
\begin{aligned}
r\,(t_{\mathrm{obs}}) &= \int_0^{t_{\mathrm{obs}}} \frac{\mathrm{d}t}{a\,(t)} \\
&= \int_{a(0)}^1 \frac{\mathrm{d}a}{a^2\,(t)\,H_{\mathrm{obs}}\sqrt{\Omega_m \frac{1}{a^3(t)} + \Omega_\Lambda}} \\
&= \frac{{}_2F_1\left(\frac{1}{3}, \frac{1}{2}; \frac{4}{3}; -\frac{\Omega_m}{a^3(0)\Omega_\Lambda}\right) - a\,(0)\,{}_2F_1\left(\frac{1}{3}, \frac{1}{2}; \frac{4}{3}; -\frac{\Omega_m}{\Omega_\Lambda}\right)}{a\,(0)\,H_{\mathrm{obs}}\sqrt{\Omega_\Lambda}}
\end{aligned}
$$

Here ${}_2F_1\,(a, b; c; z) = \frac{\Gamma(c)}{\Gamma(b)\Gamma(c-b)}\int_0^1 \frac{t^{b-1}(1-t)^{c-b-1}}{(1-tz)^a}\,\mathrm{d}t$ is a hypergeometric function. We then substitute $a\,(0) = \frac{1}{1+z}$ and finally arrive at

$$
r\,(z) = \frac{(1+z)\,{}_2F_1\left(\frac{1}{3}, \frac{1}{2}; \frac{4}{3}; -\frac{\Omega_m}{\Omega_\Lambda}(1+z)^3\right) - {}_2F_1\left(\frac{1}{3}, \frac{1}{2}; \frac{4}{3}; -\frac{\Omega_m}{\Omega_\Lambda}\right)}{H_{\mathrm{obs}}\sqrt{\Omega_\Lambda}} \tag{B2}
$$

The area of the photon sphere is then:

$$A_{\mathrm{ph}}\,(z) = 4\pi a^2\,(t_{\mathrm{obs}})\,r^2\,(z) = 4\pi r^2\,(z) \tag{B3}$$

The second sphere is the bursts sphere. It has its origin at the observer's position, and the radius the same as the photon sphere. Therefore, its area is:

$$A_{\mathrm{b}}\,(z) = 4\pi a^2\,(0)\,r^2\,(z) = \frac{4\pi r^2\,(z)}{(1+z)^2} \tag{B4}$$

It's helpful to calculate one more quantity related to the bursts sphere – the volume of the infinitesimal shell surrounding it. For that we again use the metric:

$$
\begin{aligned}
dV(z) &= -A_{\mathrm{b}}(z)\, a(0)\, dr \\
&= -A_{\mathrm{b}}(z)\, a(0) \, \frac{da}{a^2(0)\, H_{\mathrm{obs}} \sqrt{\Omega_m \frac{1}{a^3(t)} + \Omega_\Lambda}} \\
&= A_{\mathrm{b}}(z) \, \frac{\frac{1}{(1+z)^2}\, dz\,(1+z)}{H_{\mathrm{obs}} \sqrt{\Omega_m \frac{1}{a^3(t)} + \Omega_\Lambda}} \\
&= \frac{4\pi r^2(z)}{(1+z)^3} \, \frac{dz}{H_{\mathrm{obs}} \sqrt{\Omega_m (1+z)^3 + \Omega_\Lambda}}
\end{aligned}
\tag{B5}
$$

REFERENCES

Abdo, A., et al. 2009, ApJ., 706, L138

Ackermann, M., Ajello, M., Asano, K., et al. 2013, ApJS, 209, 11

Ackermann, M., et al. 2010, ApJ, 716, 1178

—. 2011, ApJ, 729, 114

—. 2012, ApJS, 203, 4

Atwood, W. B., Abdo, A. A., Ackermann, M., et al. 2009, ApJ, 697, 1071

Bloom, J. S., Frail, D., & Kulkarni, S. 2003, ApJ, 594, 674

Castignani, G., Guetta, D., Pian, E., et al. 2014, A&A, 565, A60

Cheng, L.-X., Ma, Y.-Q., Cheng, K.-S., Lu, T., Zhou, Y.-Y. 1995, A&A, 300, 746

Daigne, F., Bosnjak, Z., Dubus, G. 2011, A&A, 526, A110

Gehrels, N., & Razzaque, S. 2013, Front.Phys.China., 8, 661

Chandra, P., Frail, D.-A. 2012, ApJ, 746, 156

Ghirlanda, G., Nava, L., Ghisellini, G., et al. 2012, MNRAS, 420, 483

Goldstein, A., Connaughton, V., Briggs, M.-S., Burns, E. 2015, arXiv:1512.04464

Granot, J., Panaitescu, A., Kumar, P., Woosley, S.-E. 2002, ApJ, 570, L61

Lange, J., & Pohl, M. 2013, A&A, 551, A89

Meszaros, P., Rees, M.-J., Wijers, R.-A.-M.-J. 1998, ApJ, 499, 301

Nakamura, T., & Ioka, K. 2001, ApJ, 554, L163

Postnov, K.-A., Prokhorov, M.-E., Lipunov, V.-M. 1999, astro-ph/9908136

Racusin, J.-L., Liang, E.-W., Burrows, D.-N., Falcone, A., Sakamoto, T., Zhang, B.-B., Zhang, B., Evans, P., Osborne, J 2009, ApJ, 698, 43

Rubtsov, G., Pshirkov, M., & Tinyakov, P. 2012, Mon.Not.Roy.Astron.Soc.Lett., 421, L14

Shen, R.-F., Song, L.-M., & Li, Z. 2005, MNRAS, 362, 59

Shenoy, A., Sonbas, E., Dermer, C., et al. 2013, ApJ, 778, 3

Soderberg, A.-M. & Fenimore, E.-E. 2001, astro-ph/0103277

Tajima, H. 2009, arXiv:0907.0714

Vianello, G. 2012, eConf, C121028, 325

Wang, X.-Y., Liu, R.-Y., & Lemoine, M. ApJ, 2013, 771, L33

Wu, B., Fenimore, E. 2000, ApJ, 535, L29

Yi, T.-F., Liang, E.-W., Qin, Y.-P., & Lu, R.-J. 2006, MNRAS, 367, 1751